Published in final edited form as:
Magn Reson Med. 2008 February ; 59(2): 336–344. doi:10.1002/mrm.21467.

Evaluation of Human Brain Tumor Heterogeneity using MRI with Multiple T1-based Signal Weighting Approaches

Manus J. Donahue[1,2,3], **Jaishri O. Blakeley**[4], **Jinyuan Zhou**[1,2], **Martin G. Pomper**[1], **John Laterra**[4], and **Peter C.M. van Zijl, Ph.D**[1,2,3,*]

[1] The Russell H. Morgan Department of Radiology and Radiological Science, Neuroscience Section, Division of MR Research, Johns Hopkins University, Baltimore, MD USA

[2] F.M. Kirby Research Center for Functional Brain Imaging, Kennedy Krieger Institute, Baltimore, MD USA

[3] Department of Biophysics and Biophysical Chemistry, Johns Hopkins University, Baltimore, MD USA

[4] Department of Neurology, Johns Hopkins University, Baltimore, MD USA

Abstract

Vascular-space-occupancy (VASO)-MRI without contrast injection was explored for imaging cerebral blood volume (CBV) and tissue heterogeneity in gliomas (n=10). VASO contrast complemented contrast-enhanced T1-weighted (GAD-T1w), FLAIR and T1w Magnetization-Prepared-RApid-Gradient-Echo (MPRAGE) images. High-grade gliomas showed a VASO-outlined hyperintense zone corresponding to long-T1 regions in MPRAGE and to non-enhancing regions in GAD-T1w images. FLAIR, MPRAGE, and VASO data were used to segment tumors into multiple zones of different T1. After removal of known resection areas using pre and postsurgical MRI, the volume of overlap between the hyperintenseVASO-zone and the long-T1 MPRAGE zone correlated with that of GAD-T1w enhancement (R^2=0.99) and tumor grade. Based on these correlations, this remaining long T1 overlap area was putatively assigned to necrosis. The results suggest that this collective T1-weighted approach may provide useful information for regional assessment of heterogeneous tumors.

Keywords

Cerebral blood volume; White matter; different thresholds; tumor segmentation; MRI; VASO; MPRAGE; Gd-DTPA; FLAIR

Introduction

Despite recent treatment advances in neuro-oncology, prognosis for patients with high-grade gliomas remains poor (1–3). First-line therapy for glioma patients is neurosurgical resection and the extent of resection may impact survival (4–6). However, due to the heterogeneous, infiltrating nature of these tumors, their spatial extent is often not apparent from conventional MRI. Currently, areas targeted for resection are based largely on abnormal enhancement in T1-weighted (T1w) MRI following intravenous Gd-DTPA injection (GAD-T1w). This enhancement is attributed to blood brain barrier (BBB) leakage associated with

*Corresponding Author: Peter van Zijl, Johns Hopkins University School of Medicine, Dept. of Radiology, 217 Traylor Bldg, 720 Rutland Ave, Baltimore, MD, 21205, pvanzijl@mri.jhu.edu, Tel: 443-923-9500, Fax: 443-923-9505.

angiogenesis and capillary damage in regions of active tumor growth (7–9). However, viable tumor may extend beyond regions of contrast enhancement (8–11), while many low-grade and even some high-grade tumors may not enhance (12,13). Therefore, supplemental imaging techniques and improved processing are needed to better define regions of viable tumor and assist in diagnosis and treatment planning for glioma patients.

Angiogenesis is an important contributor to tumor growth and correlates with tumor aggressiveness (14–16). Since angiogenesis increases microvascular cerebral blood volume (CBV), CBV-imaging may provide unique insight into tumor physiology, histology and response to therapeutic agents. Both positron emission tomography (PET) and MRI-CBV methods have been employed in glioma imaging, but both require appropriately timed injection of contrast agents and subsequent post-processing (15,17), making them logistically difficult. Recently, a new MRI approach called vascular-space-occupancy (VASO) imaging was developed as a noninvasive method for detecting CBV changes accompanying neuronal activation (18). VASO is a T1-weighted MRI approach that exploits the T1 difference between blood and tissue to null intravascular blood signal, giving an image of extravascular tissue water only. While VASO has shown consistent sensitivity to CBV changes in functional MRI experiments (18–20), it has not been tested extensively in the clinic. Recently, VASO images with and without contrast were combined to quantitatively assess absolute CBV in brain tumors (21), showing promise for tumor grade assessment. However, this approach is confounded by the assumption that the administered contrast remains in the vasculature, which may not be applicable in regions of BBB breakdown. The purpose of the current study was to compare the image properties of VASO without contrast injection to GAD-T1w and FLAIR images. A high-resolution T1-weighted MRI approach called Magnetization-Prepared-RApid-Gradient-Echo (MPRAGE) was also employed to substantiate the VASO-based contrast.

VASO and MPRAGE may expand the relatively limited diagnostic specificity that traditional T1w-MRI has offered for tumor imaging. T1 values of healthy tissue at 3.0T are known to vary considerably: approximately 1209 ms for gray matter (22), 758 ms for white matter (22) and 1627 ms for blood (23). While limited data is available at 3.0T on tumor T1 values, it has been shown at 1.5T that T1 of necrotic tissue is approximately 1500–2600 ms, whereas T1 of GAD-T1w enhancing tumor is 1300–1700 ms and T1 of edematous brain is 1200–1500 ms (24–26); T1 values have also been shown to increase with tumor grade (25). In VASO, blood signal is nulled, leading to the expectation of low signal intensity in fresh tumor regions where CBV is increased. Hyperintense regions within the VASO image reflect a longer T1 (negative signal at time of blood nulling) appearing as positive signal in magnitude images (Fig. 1). In T1w MPRAGE-MRI, such areas will have lower signal intensity. These regions can reflect resection cavities as well as necrosis, but the former can generally be assigned from anatomical imaging before and after surgery. Enhancement in GAD-T1w is traditionally attributed to a disrupted BBB, due to both endothelial damage as well as pathologic angiogenesis, and occurs within tumor or around the perimeter of necrotic regions, but not within areas of edema. Our hypothesis was that, due to the appreciable differences in T1 between healthy tissue, necrosis, and edema/viable tumor, as well as the high variation in CBV within tumor regions, VASO-MRI may provide additional contrast and valuable information regarding tumor composition.

Methods

Ten patients with histologically-confirmed gliomas of varying grade were investigated: four glioblastoma multiforme (GBM, WHO grade 4), two anaplastic astrocytoma (AA, WHO grade 3), one anaplastic oligodendroglioma (AO, WHO grade 3), and three low-grade (low-grade, WHO grade 2) gliomas. Written consent was obtained from all patients prior to

involvement in this IRB-approved, HIPAA-compliant study. Rapid, moderate or slow tumor progression was tracked by the overseeing physician according to routine clinical and imaging surveillance. Rapid progression was defined as patient death within 60 days of imaging, moderate progression as visible tumor progression on MRI combined with progression of focal neurological symptoms referable to tumor and decline in performance status, and slow progression as little change in either MRI or quality of life. Because the time of diagnosis, tumor features and prior treatments varied widely between patients, tumor progression criteria provide only a rough estimation of tumor aggressiveness, which, in this pilot study, was compared qualitatively with FLAIR, MPRAGE, GAD-T1w and VASO images.

Imaging

MPRAGE, GAD-T1w, FLAIR and VASO-MRI were performed on a 3.0T MRI scanner (Philips Medical Systems, Best, The Netherlands) using body coil excitation and phased-array coil (6 channels) with sensitivity encoding (SENSE) reception. Scan parameters were *FLAIR*: 60 slices, TR/TE=11/0.12s, FOV=212, spatial resolution 0.83×0.83×2.2 mm^3, scan duration 4:57; MPRAGE *MRI*: 150 slices, 3D turbo-gradient-echo acquisition (SENSE-factor=2), TR/TE=7.9/3.7ms, FOV=256, spatial resolution 1×1×1 mm^3, scan duration 5:14; images were acquired before (T1w) and after *Gd-DTPA* injection (GAD-T1w). VASO (SENSE-factor=2): 22 slices, TR/TE =6/0.019s, three dynamics, FOV=220, in-plane spatial resolution 2.3×2.3×2.2mm^3, scan duration 3:18. In VASO, two slices were acquired in each TR and the null-time (inversion time corresponding to blood signal nulling), TI=1.086s, was centered between the two readouts.

Analysis

All images were reconstructed to a 256×256 matrix and corrected for motion and baseline drift. Whole-brain MPRAGE, GAD-T1w and FLAIR images were resliced and co-registered to the 22 VASO slices using standard algorithms established by the Oxford Centre for Functional Magnetic Resonance Imaging of the Brain (FMRIB). The FMRIB Linear Image Registration Tool (FLIRT, (27)) with a 12-parameter affine transformation and normalized mutual information cost function was used for coregistration.

Although hyper- and hypo-intensities in the different T1w images could generally be recognized by visual inspection alone, we developed a semi-automated algorithm to segment the tumor (Fig. 2). First, FMRIB's Automated Segmentation Tool (FAST) (www.fmrib.ox.ac.uk/fsl/fast) was applied to all slices in co-registered FLAIR images to obtain an outline of maximal combined tumor and edema volume. This mask was applied to MPRAGE, GAD-T1w, and VASO images and only voxels lying within this mask were analyzed. This was done by comparing intensities in the FLAIR volume with the mean signal intensity (S_h) and standard deviation (std_h) of a "seed" region-of-interest (ROI) within healthy appearing white matter. Next, for each voxel in the segmented FLAIR tumor volume, it was determined how many (n) std_h its intensity (S_i) deviated from S_h according to:

$$n=(S_i - S_h)/std_h. \quad [1]$$

Thus, n reflects how much the tumor voxel signal intensity deviates from healthy, white matter signal intensity. Separate n-maps for MPRAGE, GAD-T1w and VASO were generated. In order to perform tumor segmentation, the range of n-values corresponding to certain tumor features has to be determined. Contrast enhancement, i.e. signal increase, in GAD-T1w n-maps was defined as any voxel with $n>0$ (Fig. 2). GAD-T1w enhancement

generally occurs around necrosis and within regions of metabolically active tumor. Based on this assumption, an attempt to interprete the T1-features in MPRAGE and VASO images in terms of necrosis and viable tumor features was made with ROIs drawn in hypointense MPRAGE and hyperintense VASO n-map regions and mean n-values determined, which were labeled $n_{\max} \pm std_{\max}$ and $n_{\min} \pm std_{\min}$, respectively. Next, a region-growing algorithm was applied to determine the spatial extent of the long-T1 region. Growing began at a manual initiation point and proceeded by testing adjacent voxels to be within a certain threshold n-value. In VASO, initiation was in regions of high n-value and the threshold was $n_{\max} \pm \beta \cdot std_{\max}$. In MPRAGE, initiation corresponded to regions of low n-value and the threshold was $n_{\min} \pm \beta \cdot std_{\min}$. A threshold parameter $\beta = 1.5$ was used, but this may be varied to increase the strictness of the segmentation. As can be seen from the n-maps and original images in Fig. 2, the location of the "long-T1 zone" is visually obvious and therefore there was little bias present in the manual initiation step. We found this method to be more accurate than automated routines, however current work is focusing on development of entirely automated segmentation routines. The number of voxels from the total FLAIR lesion volume (V_{FLAIR}), the long-T1 zone as predicted by VASO (V_{VASO}^{Nec}), MPRAGE (V_{MPRAGE}^{Nec}), and both VASO *and* MPRAGE segmentation ($V_{VASO+MPRAGE}^{Nec}$) and enhancement regions in GAD-T1w ($V_{GAD-T1w}$) images were all recorded. Segmented tumor maps were generated and color-coded such that white corresponded to long-T1 regions predicted from *combined* MPRAGE and VASO segmentation, red to remaining long-T1 regions predicted by *either* MPRAGE or VASO segmentation and blue to the remaining lesion volume which was found in the FLAIR segmentation.

Finally, three of the ten patients underwent surgical resections prior to imaging. Therefore, resection cavities were identified by the overseeing radiologist from post-operative imaging as well as current MPRAGE and FLAIR images. Regions were drawn around the radiologically-confirmed resection cavities and these regions were not analyzed.

Results

Fig. 3 shows all T1w images for four representative slices for a patient with a recurrent GBM. First, notice the red arrow in the FLAIR image of Fig. 3a which identifies a small resection cavity. The resection cavity, present only on the inferior most slices, was confirmed by post-operative images and was excluded from the analysis. Second, there is great similarity between hypointensity (long T1) in the MPRAGE image and hyperintensity (long T1, low CBV) in the VASO image. These combined image features were used to assign regions of assured long T1 (white in fifth column). Third, GAD-T1w enhancement is observed around and within this region, suggesting that this long-T1 zone is surrounded by vasculature that is at least partly perfused. Fourth, a striking well-defined dark line surrounds the long-T1 region in the raw VASO image (e.g. Fig. 3c). This boundary effect is a consequence of longitudinal magnetization going from negative (zone with T1 longer than that of blood) to positive (tissue with T1 shorter than blood). A similar effect can be seen for CSF in the ventricles and for resection cavities, which both have very long T1. However, such regions were excluded from the analysis. The dark VASO line clearly demarcates the long-T1 region, unlike the MPRAGE image where the region slowly transitions to the mixed viable tumor and edema region. To illustrate the approach for region assignment, the bottom slice (d) of the MPRAGE and VASO images contains white arrows identifying confirmed long-T1 tumor zones and a yellow arrow pointing to healthy white matter. Hyperintensity in VASO (white arrows) surrounded by a dark border correspond to hypointensity in MPRAGE. Viable tissue (yellow arrow) appears bright in both MPRAGE and VASO.

Fig. 4 displays representative images for patients with varying gliomas: GBM (a), AA (b), AO (c), and low-grade (d). For the GBM (Fig. 4a) and AA (Fig. 4b) a clear central long-T1 region can be deduced from the MPRAGE and VASO images. Since GAD-T1w enhancement is robust mainly *outside* of the central, long T1 region in Fig. 4a, this tumor may consist of a region of central necrosis surrounded by a well-vascularized region of viable tumor tissue. For the AO shown in Fig. 4c, a central region of long T1 is again found, but, unlike the GBM and AA above, the region surrounding this zone does not show GAD-T1w enhancement. We hypothesize that this region may consist of a mixture of edema and infiltrating tumor. Interestingly, the MPRAGE image predicts a single, long-T1 region. However, the VASO image suggests this zoneconsists of multiple spatially-distinct regions. We conclude that the distinct regions could not be delineated in the MPRAGE image due to gradual contrast changes. However, there is an abrupt transition between negative magnetization (T1 longer than blood) and positive magnetization (T1 shorter than blood) with VASO-MRI. In the low-grade glioma (Fig. 4d), no clear hypointensity in MPRAGE or hyperintensity in VASO image is apparent.

Fig. 5 shows an interesting biopsy-confirmed mixed residual low-grade tumor with treatment effect in a patient treated with radiochemotherapy. The GAD-T1w image shows regions of contrast enhancement, which often clinically suggests tumor transformation from a low-grade to a high-grade histology. However, neither the VASO nor the MPRAGE predicts a region of long T1, suggesting that the combined MPRAGE and VASO approach may have potential for differentiating progressive or recurrent gliomas from treatment effect compared with GAD-T1w imaging. Validation studies with prospective histological sampling are planned.

Table 1 summarizes the general clinical progression information for the patients from the time of imaging as well as segmented-volume ratios with respect to the FLAIR volume, assumed to be the maximum tumor extent. Fig. 6a shows regression analysis for volume correlation between the MPRAGE and VASO-predicted long-T1 zone. This statistically significant ($p<0.01$) high correlation ($R^2=0.88$) suggests that VASO and MPRAGE provide similar information, not unexpected in view of their mechanistic origin. However, as seen in Fig. 4c, VASO contrast often gives additional or clearer information due to the black boundary outlining the long T1 region region. Increased GAD enhancement in high-grade tumors is reflected in a higher $V_{GAD-T1w}$: V_{FLAIR} ratio in GBMs (0.27±0.21) and anaplastic tumors (0.19±0.19). This ratio was only 0.03±0.02 in low-grade tumors. Similarly, the mean volume of long-T1 as predicted by combined VASO and MPRAGE was found to be elevated in high-grade tumors (Table 1). In Fig. 6b, the correlation between $V_{GAD-T1w}$: V_{FLAIR} and $V^{Nec}_{VASO+MPRAGE}$:V_{FLAIR} grouped according to tumor grade is extremely good ($R^2=0.99$), showing that the long-T1zone determined from VASO/MPRAGE, like the degree of GAD enhancement, increases with tumor grade (Fig. 6c).

Discussion

This study shows that VASO and MPRAGE MRI provide contrast complementary to GAD-T1w and FLAIR MRI for glioma imaging, Interestingly, FLAIR, VASO, and MPRAGE are all inversion-based MRI sequences. However, they each offer a range of T1w contrasts, of which a collective analysis provides information not otherwise evident. We presented a method for segmenting different T1 zones, however, visual inspection of the raw images (e.g. Figs. 3, 4) was generally sufficient for identifying different regions. This was especially evident in the VASO images, largely due to exquisite separation of positive and negative signals as based on T1 being smaller or larger than T1 of blood, respectively, which generated a well-defined black borderline around areas with T1 longer than blood T1.

The first question that arises is whether such long-T1 areas can provide any useful information for tumor diagnosis. A long T1-value could correspond to any liquid-like tissue, including necrosis, and CSF (including CSF in resection cavities). However, we removed the resection cavities based on prior knowledge from anatomical images before and after surgery. We then performed correlations between the GAD-T1w data and the VASO/MPRAGE data. The occurrence of GAD enhancement around long-T1 zones in high-grade tumors, combined with the correlation between tumor grade, GAD enhancement and the size of the long-T1 zone in VASO/MPRAGE images suggests that tumor necrosis is likely the dominant constituent in these zones. This possible explanation is supported by absence of similar long-T1 zones in low-grade tumors. The assignment of the remaining tumor regions is more difficult. In all of the above cases, the VASO images appear dark in the tumor indicating that VASO may not qualify for separating this residual area into edema or viable tumor due to a comparable T1-range for these two tissue types.

The preliminary findings in this paper have several clinical implications. First, in terms of pragmatics, VASO-MRI and MPRAGE-MRI do not require contrast injection, making them easily incorporable into existing protocols and, for VASO, a good alternative to CBV imaging using dynamic GAD approaches. This is important considering potential risks of contrast administration in patients with renal failure including nephrogenic systemic fibrosis and fibrosing dermopathy. Obviously, much more validation is needed before elimination of GAD approaches can be suggested, as they are currently well validated and essential for clinical evaluation of brain tumors. Second, VASO provides information on the physiological parameter, CBV (18). Therefore, novel therapeutic strategies which focus on growth factors associated with vascular proliferation (14,16) may incorporate VASO as a method for screening antiangiogenic agents and tracking therapy response in regions of high vascularity (28–30). VASO-MRI is additionally appealing since it does not require timed bolus contrast injection. A current disadvantage of VASO-MRI is that the T1 of edema and viable tumor may mimic T1 of blood, complicating delineation. However, dynamic experiments (e.g. using a breath-hold stimulus) may aid in distinguishing compartments.

Regression analysis showed a significant correlation between V^{Nec}_{MPRAGE} and V^{Nec}_{VASO} (Fig. 6) and increased $V^{Nec}_{MPRAGE}:V_{FLAIR}$ and $V^{Nec}_{VASO}:V_{FLAIR}$ in high-grade tumors compared with lower-grade tumors. Thus, VASO and MPRAGE provide similar information regarding features of high-grade tumors, but the data indicate that combining the two methodologies provides the most reliable data for tumor grading. This is illustrated for one low-grade tumor in Table 1 (case 8), where the MPRAGE and VASO images individually predicted possible high-grade, but when MPRAGE and VASO segmentation was combined, the result correctly predicted a low-grade tumor. Putative necrotic zones were found more frequently in high-grade tumors, correlating with increased GAD enhancement. However, GAD enhancement is not specific to either necrotic zones or viable tumor regions. Error bars (standard error) were smaller for the combined VASO and MPRAGE approach compared with GAD-T1w enhancement, suggesting that detection of the presence of necrotic zones may ultimately be a reliable measure of tumor grade. Although these initial results are intriguing, the conclusions are limited since prospective pathologic sampling for direct radiopathologic correlation was not obtained and other variables which may alter imaging features (i.e. glucocorticoids, prior therapies) were not controlled.

One may notice that the $V^{Nec}_{VASO+MPRAGE}:V_{FLAIR}$ ratios appear small, even in high-grade tumors. The reason is that the values in Table 1 reflect the entire, 22-slice tumor volume, while the slices presented in the figures are only representative slices traversing the center of the tumor. Also, the semi-automated segmentation routine was based on a region growing algorithm with hand-selected initiation points. While the location of the initiation points is

readily apparent from the figures, current work is aimed at developing a reliable, fully automated routine.

These preliminary data suggest that VASO-MRI is feasible in glioma imaging and provides contrast that complements conventional FLAIR and GAD-T1w approaches. When combining the three inversion-based MRI sequences (FLAIR, VASO, and MPRAGE), clear trends regarding T1 zones were found, which were interpreted in terms of necrosis and viable tumor or edema locations. This inclusion of additional MRI sequences in the tumor imaging protocol was possible because MRI acquisitions can be played out in a shorter time at high field strength without loss of signal-to-noise (here four scans in approximately 15 minutes). We believe that inclusion of VASO and MPRAGE to brain tumor protocols may be useful for surgical and radiation treatment planning, and assessing tumor response to antiangiogenic therapies. Future validation studies to prospectively correlate VASO and MPRAGE findings with pathology and clinical course are planned.

Conclusions

Multiple T1-weighted MRI approaches were combined to segment tumors into separate T1-zones. VASO-MRI provided novel, clear information due to the black borderline which surrounded the long T1-zone. The presence of an area of T1 longer than blood water T1 correlated with tumor grade and the volume of enhancement in GAD-enhanced MRI. This was used to tentatively assign the long-T1 zone to tumor necrosis and the remainder of the volume to viable tumor or edema.

Acknowledgments

Grant support: NIH-NCRR P41-RR15241, NIH-NIBIB EB002666

The authors are grateful to Richard Edden, Terri Brawner, Kathleen Kahl, Ivana Kusevic, Craig Jones, Seth Smith, and Joe Gillen for experimental assistance. Dr. van Zijl is a paid lecturer for Philips Medical Systems. This arrangement has been approved by Johns Hopkins University in accordance with its conflict of interest policies.

References

1. Kaba SE, Kyritsis AP. Recognition and management of gliomas. Drugs 1997;53(2):235–244. [PubMed: 9028743]
2. Palanichamy K, Erkkinen M, Chakravarti A. Predictive and prognostic markers in human glioblastomas. Curr Treat Options Oncol 2006;7(6):490–504. [PubMed: 17032561]
3. Group USCSW. United States Cancer Statistics: 1999–2001 Incidence and Mortality Web-based Report Version. Department of Health and Human Services CfDCaP, and National Cancer Institute; 2004.
4. Laws ER, Parney IF, Huang W, Anderson F, Morris AM, Asher A, Lillehei KO, Bernstein M, Brem H, Sloan A, Berger MS, Chang S. Survival following surgery and prognostic factors for recently diagnosed malignant glioma: data from the Glioma Outcomes Project. J Neurosurg 2003;99(3):467–473. [PubMed: 12959431]
5. Devaux BC, O'Fallon JR, Kelly PJ. Resection, biopsy, and survival in malignant glial neoplasms. A retrospective study of clinical parameters, therapy, and outcome. J Neurosurg 1993;78(5):767–775. [PubMed: 8468607]
6. Kowalczuk A, Macdonald RL, Amidei C, Dohrmann G 3rd, Erickson RK, Hekmatpanah J, Krauss S, Krishnasamy S, Masters G, Mullan SF, Mundt AJ, Sweeney P, Vokes EE, Weir BK, Wollman RL. Quantitative imaging study of extent of surgical resection and prognosis of malignant astrocytomas. Neurosurgery 1997;41(5):1028–1036. discussion 1036–1028. [PubMed: 9361056]
7. Hawighorst H, Schreiber W, Knopp MV, Essig M, Engenhart-Cabilic R, Brix G, van Kaick G. Macroscopic tumor volume of malignant glioma determined by contrast-enhanced magnetic

resonance imaging with and without magnetization transfer contrast. Magn Reson Imaging 1996;14(10):1119–1126. [PubMed: 9065901]

8. Felix R, Schorner W, Laniado M, Niendorf HP, Claussen C, Fiegler W, Speck U. Brain tumors: MR imaging with gadolinium-DTPA. Radiology 1985;156(3):681–688. [PubMed: 4040643]
9. Pronin IN, Holodny AI, Petraikin AV. MRI of high-grade glial tumors: correlation between the degree of contrast enhancement and the volume of surrounding edema. Neuroradiology 1997;39(5): 348–350. [PubMed: 9189880]
10. Brant-Zawadzki M, Norman D, Newton TH, Kelly WM, Kjos B, Mills CM, Dillon W, Sobel D, Crooks LE. Magnetic resonance of the brain: the optimal screening technique. Radiology 1984;152(1):71–77. [PubMed: 6729138]
11. Earnest, Ft; Kelly, PJ.; Scheithauer, BW.; Kall, BA.; Cascino, TL.; Ehman, RL.; Forbes, GS.; Axley, PL. Cerebral astrocytomas: histopathologic correlation of MR and CT contrast enhancement with stereotactic biopsy. Radiology 1988;166(3):823–827. [PubMed: 2829270]
12. Aronen HJ, Gazit IE, Louis DN, Buchbinder BR, Pardo FS, Weisskoff RM, Harsh GR, Cosgrove GR, Halpern EF, Hochberg FH, et al. Cerebral blood volume maps of gliomas: comparison with tumor grade and histologic findings. Radiology 1994;191(1):41–51. [PubMed: 8134596]
13. Knopp EA, Cha S, Johnson G, Mazumdar A, Golfinos JG, Zagzag D, Miller DC, Kelly PJ, Kricheff. Glial neoplasms: dynamic contrast-enhanced T2*-weighted MR imaging. Radiology 1999;211(3):791–798. [PubMed: 10352608]
14. Reijneveld JC, Voest EE, Taphoorn MJ. Angiogenesis in malignant primary and metastatic brain tumors. J Neurol 2000;247(8):597–608. [PubMed: 11041327]
15. Aronen HJ, Pardo FS, Kennedy DN, Belliveau JW, Packard SD, Hsu DW, Hochberg FH, Fischman AJ, Rosen BR. High microvascular blood volume is associated with high glucose uptake and tumor angiogenesis in human gliomas. Clin Cancer Res 2000;6(6):2189–2200. [PubMed: 10873068]
16. Folkman J. Angiogenesis in cancer, vascular, rheumatoid and other disease. Nat Med 1995;1(1): 27–31. [PubMed: 7584949]
17. Aronen HJ, Glass J, Pardo FS, Belliveau JW, Gruber ML, Buchbinder BR, Gazit IE, Linggood RM, Fischman AJ, Rosen BR, et al. Echo-planar MR cerebral blood volume mapping of gliomas. Clinical utility Acta Radiol 1995;36(5):520–528.
18. Lu H, Golay X, Pekar JJ, Van Zijl PC. Functional magnetic resonance imaging based on changes in vascular space occupancy. Magn Reson Med 2003;50(2):263–274. [PubMed: 12876702]
19. Lu H, Basso G, Serences JT, Yantis S, Golay X, van Zijl PC. Retinotopic mapping in the human visual cortex using vascular space occupancy-dependent functional magnetic resonance imaging. Neuroreport 2005;16(15):1635–1640. [PubMed: 16189469]
20. Lu H, Golay X, Pekar JJ, Van Zijl PC. Sustained poststimulus elevation in cerebral oxygen utilization after vascular recovery. J Cereb Blood Flow Metab 2004;24(7):764–770. [PubMed: 15241184]
21. Lu, H.; Pollack, E.; Young, R.; Babb, JS.; Johnson, G.; Jensen, JH.; Helpern, JA.; Law, M. Predicting Grade of Cerebral Glioma Using Vascular-Space-Occupancy (VASO) MRI. International Society for Magnetic Resonance in Medicine; 2006 May 11; Seattle, WA USA. 2006. p. 168
22. Lu H, Nagae-Poetscher LM, Golay X, Lin D, Pomper M, van Zijl PC. Routine clinical brain MRI sequences for use at 3.0 Tesla. J Magn Reson Imaging 2005;22(1):13–22. [PubMed: 15971174]
23. Lu H, Clingman C, Golay X, van Zijl PC. Determining the longitudinal relaxation time (T1) of blood at 3.0 Tesla. Magn Reson Med 2004;52(3):679–682. [PubMed: 15334591]
24. Andersen C, Haselgrove JC, Doenstrup S, Astrup J, Gyldensted C. Resorption of peritumoural oedema in cerebral gliomas during dexamethasone treatment evaluated by NMR relaxation time imaging. Acta Neurochir (Wien) 1993;122(3–4):218–224. [PubMed: 8372711]
25. Bastin ME, Sinha S, Whittle IR, Wardlaw JM. Measurements of water diffusion and T1 values in peritumoural oedematous brain. Neuroreport 2002;13(10):1335–1340. [PubMed: 12151798]
26. Andersen C, Jensen FT. Differences in blood-tumour-barrier leakage of human intracranial tumours: quantitative monitoring of vasogenic oedema and its response to glucocorticoid treatment. Acta Neurochir (Wien) 1998;140(9):919–924. [PubMed: 9842429]

27. Jenkinson M, Smith S. A global optimisation method for robust affine registration of brain images. Med Image Anal 2001;5(2):143–156. [PubMed: 11516708]

28. Batchelor TT, Sorensen AG, di Tomaso E, Zhang WT, Duda DG, Cohen KS, Kozak KR, Cahill DP, Chen PJ, Zhu M, Ancukiewicz M, Mrugala MM, Plotkin S, Drappatz J, Louis DN, Ivy P, Scadden DT, Benner T, Loeffler JS, Wen PY, Jain RK. AZD2171, a pan-VEGF receptor tyrosine kinase inhibitor, normalizes tumor vasculature and alleviates edema in glioblastoma patients. Cancer Cell 2007;11(1):83–95. [PubMed: 17222792]

29. Cao C, Albert JM, Geng L, Ivy PS, Sandler A, Johnson DH, Lu B. Vascular endothelial growth factor tyrosine kinase inhibitor AZD2171 and fractionated radiotherapy in mouse models of lung cancer. Cancer Res 2006;66(23):11409–11415. [PubMed: 17145887]

30. Nakamura K, Taguchi E, Miura T, Yamamoto A, Takahashi K, Bichat F, Guilbaud N, Hasegawa K, Kubo K, Fujiwara Y, Suzuki R, Kubo K, Shibuya M, Isae T. KRN951, a highly potent inhibitor of vascular endothelial growth factor receptor tyrosine kinases, has antitumor activities and affects functional vascular properties. Cancer Res 2006;66(18):9134–9142. [PubMed: 16982756]

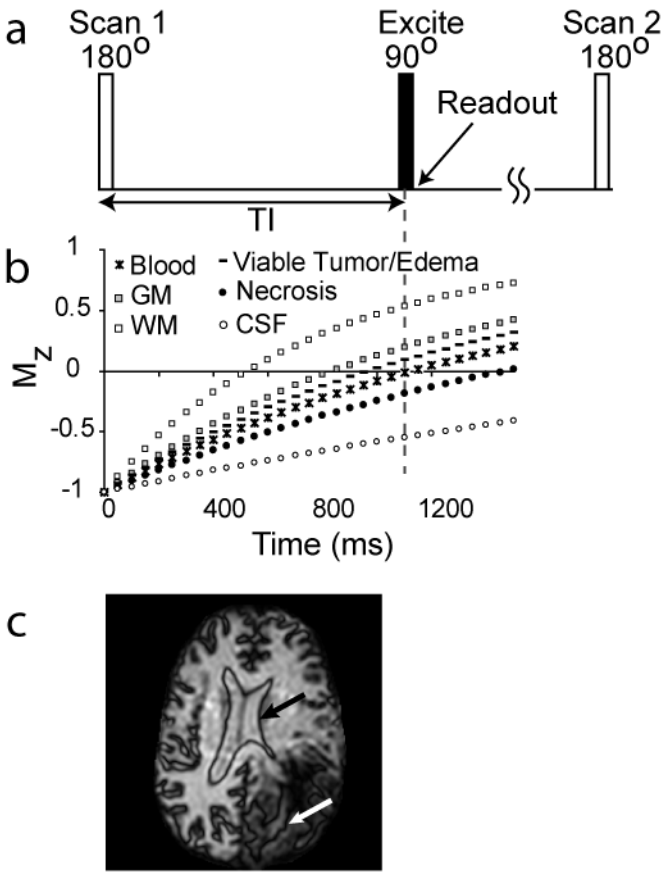

Figure 1.

The VASO pulse sequence (a) consists of a spatially nonselective adiabatic inversion followed by imaging at an inversion time (TI) when blood water magnetization is nulled. The T1 recovery curves for healthy gray matter (GM) and white matter (WM), estimated viable tumor and edema, blood, predicted necrosis, and CSF are shown in (b). At the TI for blood nulling, healthy WM signals are positive, while areas with viable tumor (including some edema and increased CBV) generally appear dark, although this may vary with individual and tumor grade. Necrosis and CSF signals (including cavity fluid) are negative due to long T1 here. Therefore, when magnitude VASO images are displayed, a dark line will surround the CSF/parenchyma boundary (c, black arrow) as well as the necrosis/parenchyma boundary (c, white arrow).

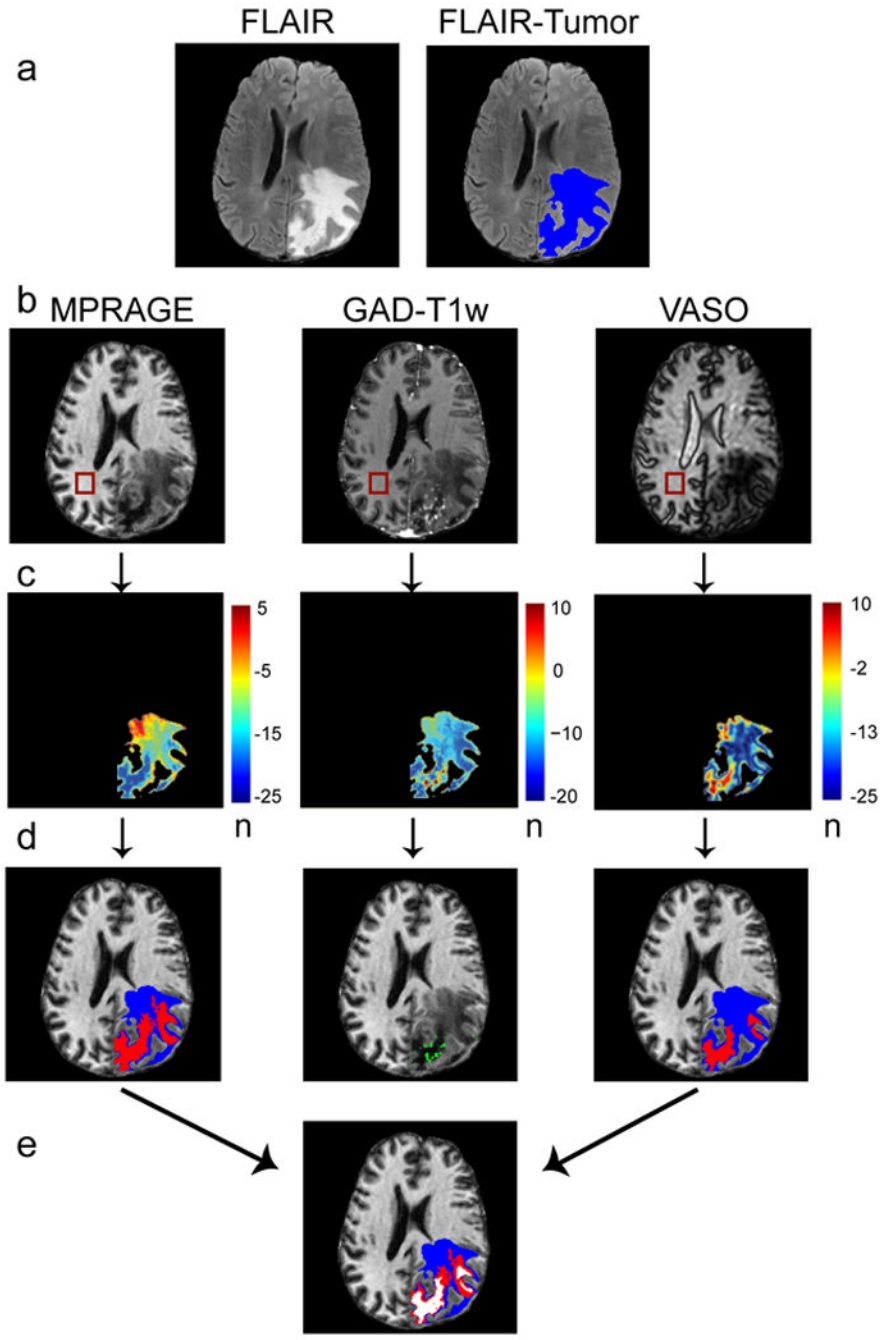

Figure 2.

Method for automated tumor segmentation. First row, the maximum area of tumor plus edema is identified by segmenting the FLAIR image (a, blue). Second row, a corresponding ROI is drawn within healthy white matter in the MPRAGE, GAD-T1w and VASO images and the mean signal intensities and standard deviations are recorded (b). Third row, *n*-maps are generated that reflect the number (n) of standard deviations each FLAIR-masked tumor voxel differs from mean healthy white matter signal intensity (c). Fourth row, thresholds and region growing procedures are applied to segment regions of abnormal intensity (d). The VASO and MPRAGE images are segmented into long-T1 (red) and remaining volume from FLAIR (blue). Fifth row, for improved consistency, overlapping regions in the MPRAGE

and VASO image are identified for a final segmentation of predicted-long-T1 (white) and surrounding regions (e).

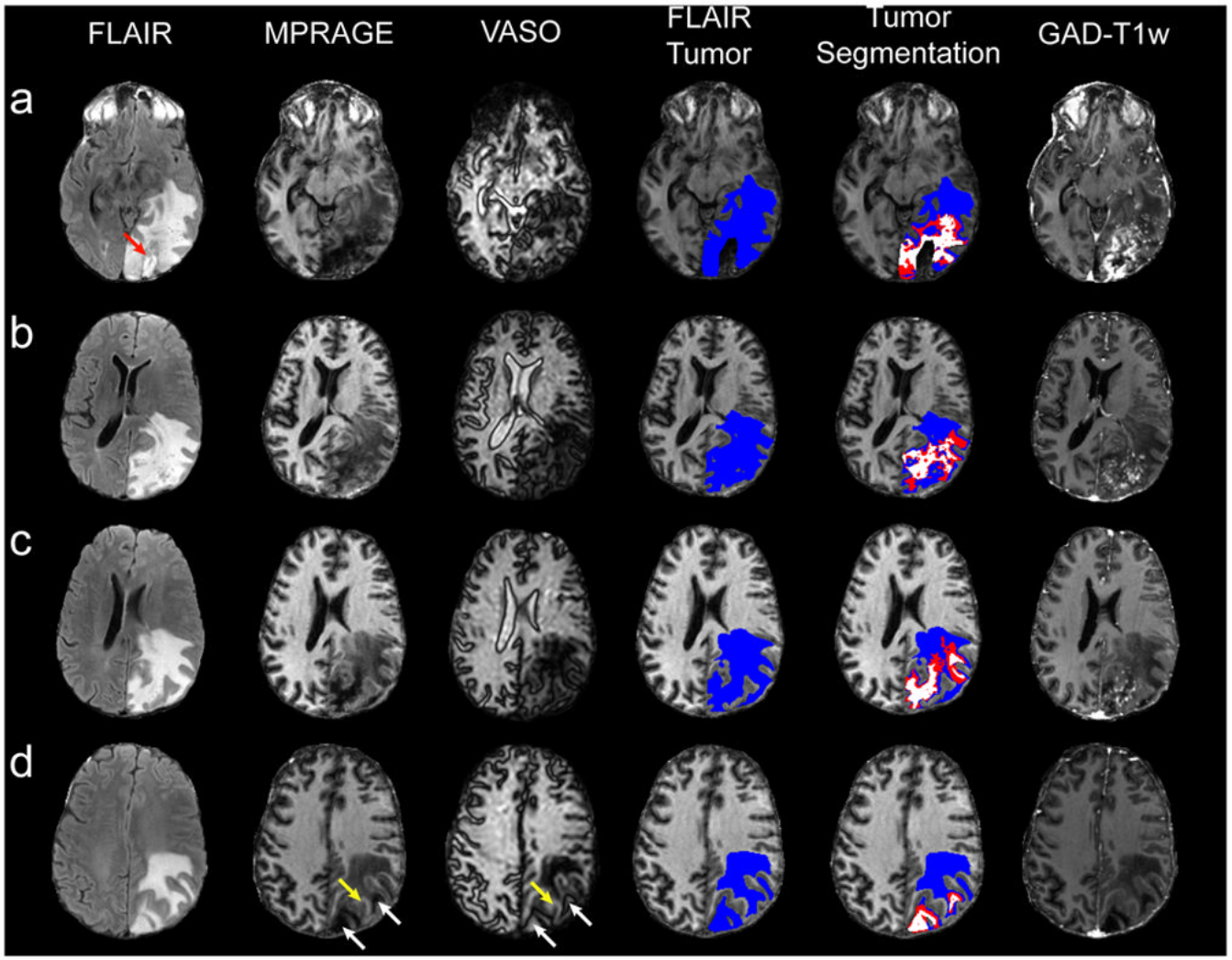

Figure 3.
Four representative slices from a single patient with a GBM. Notice the red arrow pointing to the exluded, radiologically-confirmed resection cavity in the first FLAIR image (a). Volume segmentation for the maximum tumor area (FLAIR, blue) and long-T1 zone (combined VASO/MPRAGE, white) is shown in the fourth and fifth columns. The red region represents long-T1 predicted by either MPRAGE or VASO, but not both. In (d), white arrows on the MPRAGE and VASO images point to long-T1 tumor sections, putatively assigned to necrosis (see discussion) whereas yellow arrows point to healthy white matter.

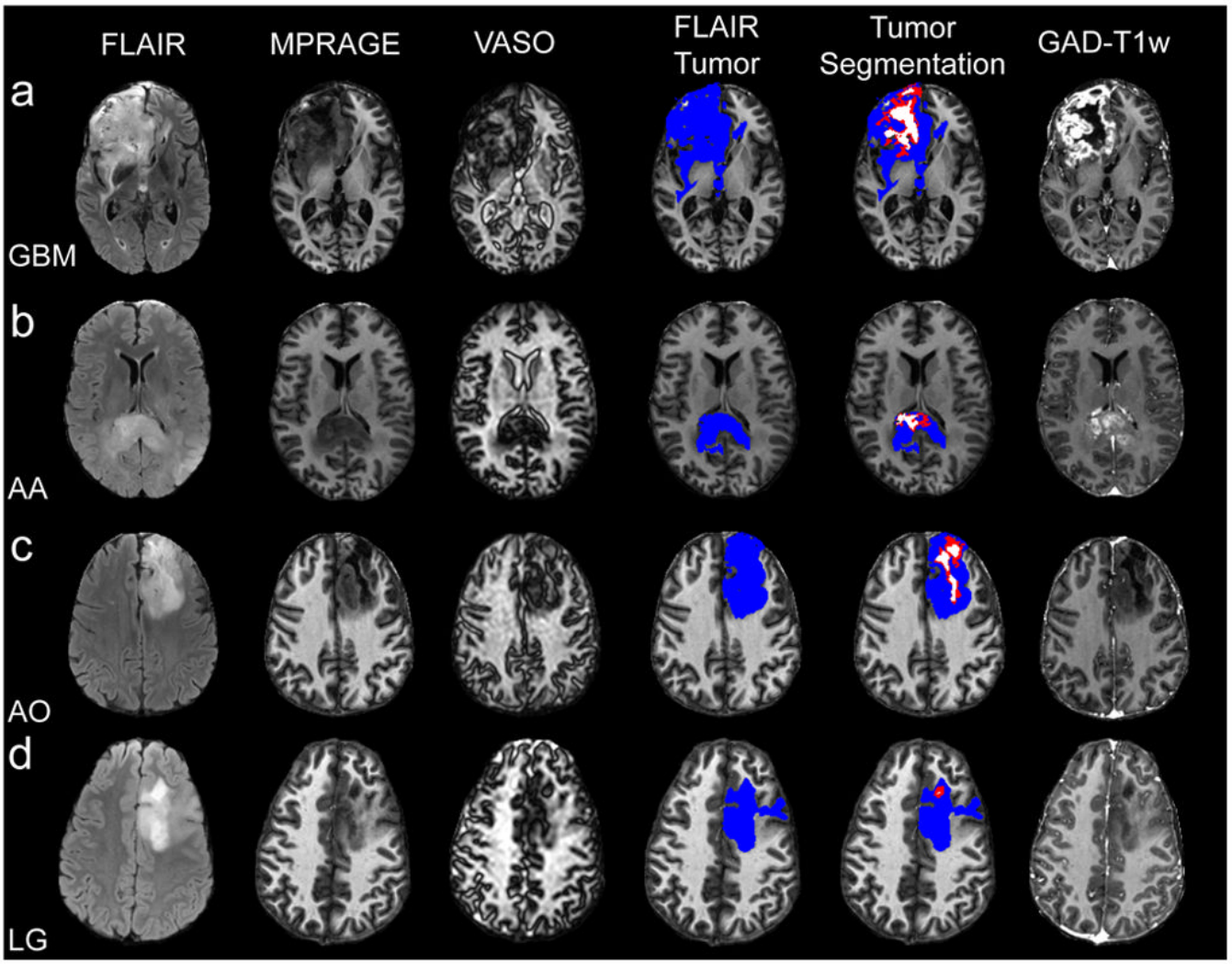

Figure 4.
One representative slice for a GBM (a), AA (b), AO (c) and low-grade (LG) (c). Long-T1 zones exist, to varying spatial extents, in the high-grade tumors, with negligible detectable long-T1 zone in the low-grade tumor. Notice the dark boundary surrounding the VASO hyperintense (long-T1) zone corresponding to a non-enhancing central tumor area, which is putatively assigned to necrosis (see discussion).

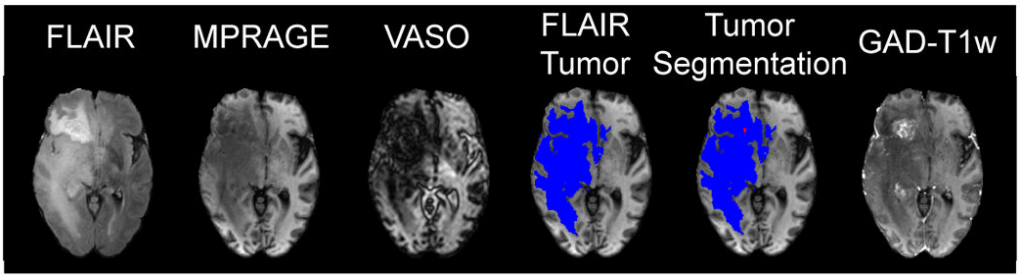

Figure 5.
A biopsy-confirmed low-grade tumor with treatment effects. Notice that the GAD-T1w image shows regions of enhancement, suggesting a possible high-grade tumor. However, the VASO and MPRAGE images show no clear regions of hypo- or hyper-intensity, implying that there is no necrotic zone and implicating the true low-grade diagnosis.

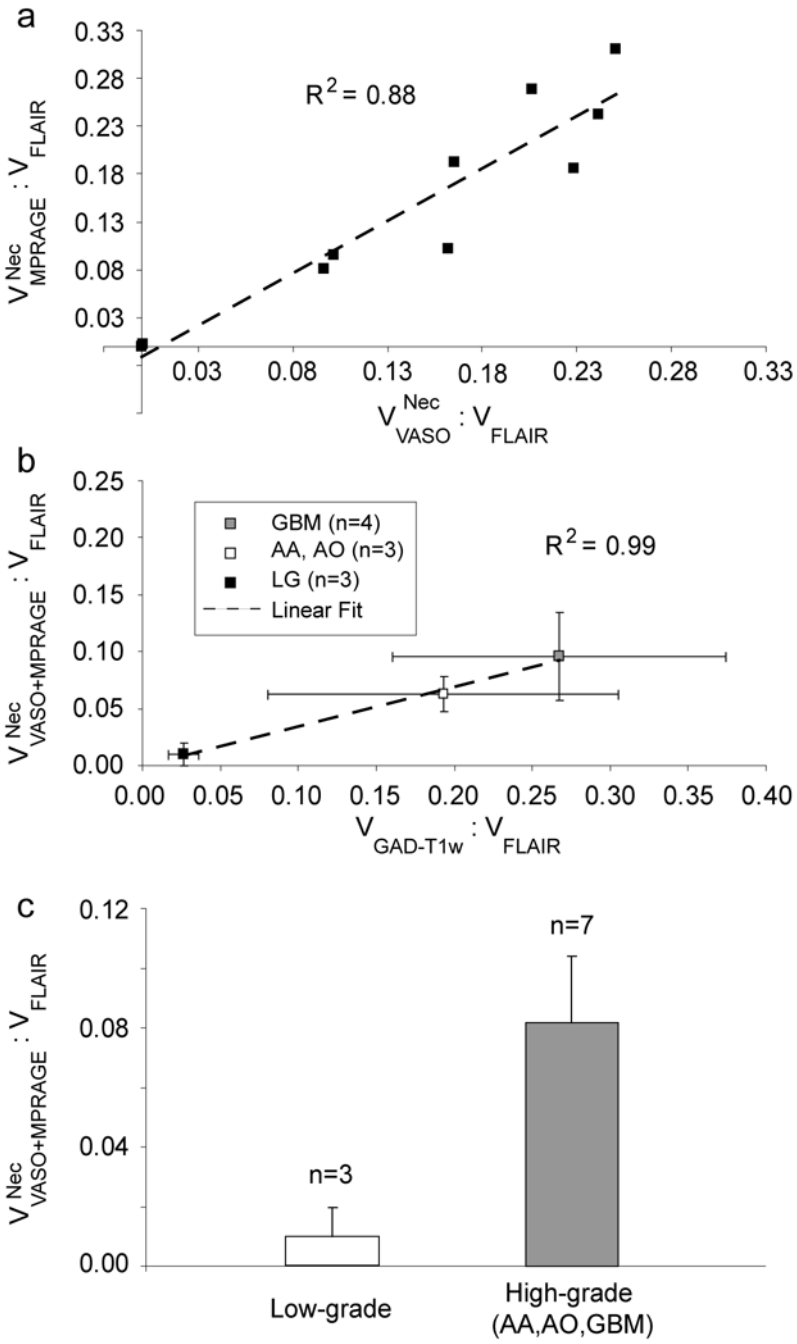

Figure 6.

(a) Regression analysis for MPRAGE and VASO long-T1 zones. MPRAGE and VASO predict similar long-T1 volumes, an observation significant at $p<0.01$. A strong correlation between GAD-T1w volumes and combined predicted MPRAGE and VASO long-T1 volume exists (b), which, on average, also increases with tumor grade (c). Therefore, VASO and MPRAGE approaches may provide a method for noninvasively determining tumor grade. Error bars represent standard error.

Table 1

Patient Information and tumor volume ratios[#]

Patient	Diagnosis	Status	$V_{GAD-T1w}:V_{FLAIR}$	$V^{Nec}_{VASO}:V_{FLAIR}$	$V^{Nec}_{MPRAGE}:V_{FLAIR}$	$V^{Nec}_{VASO+MPRAGE}:V_{FLAIR}$
1	GBM	Rapid	0.18	0.25	0.31	0.18
2	GBM	Slow	0.46	0.21	0.27	0.14
3	GBM	Moderate	0.01	0.10	0.08	0.05
4[*]	GBM	Moderate	0.42	0.16	0.10	0.01
Mean			**0.27**	**0.18**	**0.19**	**0.10**
STD			**0.21**	**0.07**	**0.12**	**0.08**
5	AA	Rapid	0.41	0.23	0.19	0.07
6	AA	Rapid	0.14	0.10	0.09	0.03
7	AO	Slow	0.03	0.17	0.19	0.09
Mean			**0.19**	**0.17**	**0.16**	**0.06**
STD			**0.19**	**0.06**	**0.05**	**0.03**
8[**]	LG	N/A	0.01	0.24	0.24	0.03
9	LG	Slow	0.04	0.00	0.00	0.00
10	LG	Slow	0.03	0.00	0.00	0.00
Mean			**0.03**	**0.08**	**0.08**	**0.01**
STD			**0.02**	**0.14**	**0.14**	**0.02**

[#]Ratios of segments with respect to total tumor volume based on FLAIR imaging

[*]Noticable patient motion between scans.

[**]Both MPRAGE and VASO indicate a possible necrotic region with long T1, but there is no overlap, leading to the correct diagnosis of low-grade.

Key: GBM=glioblastoma multiforme, AA= anaplastic astrocytoma, AO=anaplastic oligodendroglioma, LG=low-grade.